

# A mechanism for phase separation in copper oxide superconductors

A.O. Sboychakov,<sup>1,2</sup> Sergey Savel'ev,<sup>1,3</sup> A.L. Rakhmanov,<sup>1,2,3</sup> K.I. Kugel,<sup>2,3</sup> and Franco Nori<sup>1,4</sup>

<sup>1</sup>Frontier Research System, The Institute of Physical and Chemical Research (RIKEN), Wako-shi, Saitama, 351-0198, Japan

<sup>2</sup>Institute for Theoretical and Applied Electrodynamics Russian Academy of Sciences, 125412 Moscow, Russia

<sup>3</sup>Department of Physics, Loughborough University, Loughborough LE11 3TU, United Kingdom

<sup>4</sup>Center for Theoretical Physics, CSCS, Department of Physics,  
University of Michigan, Ann Arbor, MI 48109-1040, USA

(Dated: November 4, 2018)

A two-band Hubbard model is used to describe the band structure and phase separation (PS) in multiband superconductors, especially in cuprates. We predict a large peak in the density of states at the Fermi level in the case of optimum doping, corresponding to the minimum energy difference between the centers of two hole bands. For strong interband hybridization, a metal-insulator transition occurs near this optimum doping level. We suggest a mechanism of PS related to the redistribution of holes between two Hubbard bands rather than to the usual antiferromagnetic correlations. We show that the critical superconducting temperature  $T_c$  can be about its maximum value within a wide range of doping levels due to PS.

PACS numbers: 74.72.-h, 71.27.+a, 64.75.+g

Nanoscale spatial variations in the electronic characteristics of different high- $T_c$  superconductors have been commonly observed in the form of stripes [1], granular droplet-like structures [2], four-unit-cell periodic (checkerboard) patterns [3], or even more intricate arrangements [4]. Several theoretical models also suggest inhomogeneous electron structure in superconducting cuprates and related materials [5, 6, 7, 8]. Moreover, the phenomenon of self-organized electron inhomogeneity or phase separation (PS) is common to many strongly correlated electron systems [1, 9]. For example, PS in the form of droplets, stripes, and checkerboard patterns has been observed in doped magnetic oxides (manganites) [1]. Many theoretical approaches [1, 7, 8, 9] explain PS as a result of the competition between electron localization, due to antiferromagnetic correlations, and delocalization in the non-magnetic (or ferromagnetic) regions.

Here we consider an alternative mechanism (*without* antiferromagnetic correlations) for the PS arising in a Hubbard model with two (or more) bands. Even though this model is commonly used to describe high- $T_c$  superconductors [10], PS has not been studied using such an approach. The two-band Hubbard model allows us to describe PS of the droplet type (including the droplet size) observed in experiments (see, e.g., [2, 4]). In contrast to the usual mechanism, based on antiferromagnetic correlations, here we show that our proposed mechanism of PS gives rise to a density of states (DOS) at the Fermi level, which corresponds to the optimum doping in one of the phases. This results in a weak variance of the critical temperature within a broad doping range, as observed in experiments. The number of charge carriers in superconducting cuprates is not directly determined by the doping level and can depend on temperature [10, 11]. This fundamental problem can be also understood in the framework of two-band models [11].

*Two-band Hubbard model.*— The usual model used to describe superconducting cuprates is based on the Hubbard Hamiltonian with three bands: Cu( $3d$ ), O( $2p_x$ ), and O( $2p_y$ ) [10]. In earlier studies, this Hamiltonian was reduced to an effective single-band Hubbard Hamiltonian (see, e.g., [10, 12]). However, recent computations (see, e.g., [13, 14]) show that two distinguishable Cu-O bond lengths in the CuO<sub>6</sub> octahedron, and the direct tunnelling of holes between the oxygen atoms lead to the effective two-band Hubbard Hamiltonian [14]:

$$\mathcal{H} = - \sum_{\langle \mathbf{nm} \rangle \alpha \beta \sigma} t^{\alpha\beta} a_{\mathbf{n}\alpha\sigma}^\dagger a_{\mathbf{m}\beta\sigma} - \sum_{\mathbf{n}\alpha\sigma} (\mu + \epsilon_\alpha) n_{\mathbf{n}\alpha\sigma} + \frac{1}{2} \sum_{\mathbf{n}\alpha,\sigma} U^\alpha n_{\mathbf{n}\alpha\sigma} n_{\mathbf{n}\alpha\bar{\sigma}} + \frac{U'}{2} \sum_{\mathbf{n}\alpha,\sigma\sigma'} n_{\mathbf{n}\alpha\sigma} n_{\mathbf{n}\bar{\alpha}\sigma'} . \quad (1)$$

Here,  $a_{\mathbf{n}\alpha\sigma}^\dagger$  and  $a_{\mathbf{n}\alpha\sigma}$  are the creation and annihilation operators for holes in the state  $\alpha = \{p, d\}$  at site  $\mathbf{n}$  with spin projection  $\sigma$  ( $\bar{\alpha}, \bar{\sigma}$  denote not- $\alpha$  and not- $\sigma$ ), the symbol  $\langle \dots \rangle$  denotes a summation over the nearest sites,  $\mu$  is the chemical potential,  $\epsilon_d$  is the energy difference between the centers of the  $d$  and  $p$  bands and  $\epsilon_p = 0$ . The first term in Eq. (1) is the kinetic energy of the conduction holes, the second term is due to the chemical potential and the shift between the centers of  $d$  and  $p$  bands. The last two terms correspond, respectively, to the intra- and interband on-site Coulomb repulsion. In agreement to Ref. 14, we assume that the Coulomb interaction is strong enough, that is  $U^\alpha, U' \gg t^{\alpha\beta}, \epsilon_d$ . Applying the mean field (so-called Hubbard I) approximation,  $\langle \hat{T} a_{\mathbf{m}\alpha\sigma}(t) n_{\mathbf{n}\beta\sigma'}(t) a_{\mathbf{n}\alpha\sigma}^\dagger(t_0) \rangle \rightarrow \langle n_{\mathbf{n}\beta\sigma'} \rangle \langle \hat{T} a_{\mathbf{m}\alpha\sigma}(t) a_{\mathbf{n}\alpha\sigma}^\dagger(t_0) \rangle$  ( $\hat{T}$  is time-ordering opera-

tor), for Hamiltonian (1), we derive the relationship

$$(\omega + \mu + \epsilon^\alpha) G_{\alpha\beta}(\omega, \mathbf{k}) = g_\alpha \left( 1 + \sum_\gamma \varepsilon^{\alpha\gamma}(\mathbf{k}) G_{\gamma\beta}(\omega, \mathbf{k}) \right), \quad (2)$$

for the one-particle Green's functions  $G_{\alpha\beta, \sigma\sigma'}(\mathbf{n} - \mathbf{n}_0, t - t_0) = -i \langle \hat{T} a_{\mathbf{n}\alpha\sigma}(t) a_{\mathbf{n}_0\beta\sigma'}^\dagger(t_0) \rangle$  in the frequency-momentum  $(\omega, \mathbf{k})$  representation; where  $g_\alpha = 1 - n_{\bar{\alpha}} - n_\alpha/2$ . The form of the function  $\varepsilon^{\alpha\beta}(\mathbf{k})$  depends on the symmetry of the crystal lattice. We analyze here a simple cubic lattice. In this case, we obtain  $\varepsilon^{\alpha\beta}(\mathbf{k}) = w^{\alpha\beta} \zeta(\mathbf{k})$ ,  $w^{\alpha\beta} = z t^{\alpha\beta}$ , and  $\zeta(\mathbf{k}) = -[\cos(k_1 d) + \cos(k_2 d) + \cos(k_3 d)]/3$ , where  $d$  is the lattice constant. Below we consider a purely paramagnetic state, that is,  $n_{\alpha\uparrow} = n_{\alpha\downarrow} = n_\alpha/2$ , and neglect the values  $\langle a_\alpha^\dagger a_{\bar{\alpha}} \rangle$ . Note, however, that the latter assumption does not affect much the obtained results [15].

Relationship (2) is the linear set of the equations for  $G_{\alpha\beta}$ , which can be easily solved. The calculated Green's functions determine the DOS and the energy of the system. Following this approach, we derive the DOS,  $\rho_{\alpha\beta}(E) = -\pi^{-1} \int d^3\mathbf{k}/(2\pi)^3 \text{Im}[G_{\alpha\beta}(\omega + i0, \mathbf{k})]_{\omega+\mu=E}$ , in the form

$$\rho_{\alpha\beta}(E) = \sqrt{g_\alpha g_\beta} \sum_{j=\pm 1} \int \frac{d^3\mathbf{k}}{(2\pi)^3} v_\alpha^j v_\beta^j \delta(E - \bar{\varepsilon}_j(\mathbf{k})), \quad (3)$$

where  $\bar{\varepsilon}_j(\zeta(\mathbf{k}))$  and  $v_\alpha^j(\zeta(\mathbf{k}))$  are the eigenvalues and eigenvectors of the matrix  $\bar{\varepsilon}^{\alpha\beta}(\zeta) = \sqrt{g_\alpha g_\beta} w^{\alpha\beta} \zeta - \delta_{\alpha\beta} \epsilon^\alpha$ . Solving this eigenvalue problem, we obtain the energy spectrum  $\bar{\varepsilon}_j(\mathbf{k})$  of holes in two new bands (labelled by  $j = \pm 1$ ) and coefficients  $v_\alpha^j$  determining the transformation from  $p$  and  $d$  holes to the quasiparticles in these bands

$$\bar{\varepsilon}_j(\zeta(\mathbf{k})) = \frac{1}{2} \left\{ (\bar{w}^{aa} + \bar{w}^{bb})\zeta - \epsilon - j \sqrt{[(\bar{w}^{aa} - \bar{w}^{bb})\zeta + \epsilon]^2 + 4(\bar{w}^{ab})^2} \right\}, \quad (4)$$

$$v^j(\zeta) = \frac{1}{\sqrt{[\bar{w}^{aa}\zeta - \bar{\varepsilon}_j]^2 + (\bar{w}^{ab})^2 \zeta^2}} \begin{pmatrix} -\bar{w}^{ab}\zeta \\ \bar{w}^{aa}\zeta - \bar{\varepsilon}_j \end{pmatrix}, \quad (5)$$

where  $\bar{w}^{\alpha\beta} = \sqrt{g_\alpha g_\beta} w^{\alpha\beta}$ . In contrast to  $p$  and  $d$  holes with short lifetime due to interband transitions, new quasiparticles with spectrum (4) have a longer lifetime and are scattered by, e.g., phonons and impurities. The transformation performed above is similar to the well-known Zhang-Rice derivation of the single-band effective Hamiltonian if  $t_{pp} = 0$  [12]. We denote the lower band as  $j = 1$  and the upper one as  $j = -1$ . We can write  $\rho_{\alpha\beta}$  using the dimensionless DOS  $\rho_0(E') = \int \delta(E' - \zeta(\mathbf{k})) d^3\mathbf{k}/(2\pi)^3$  of uncorrelated electrons,

$$\rho_{\alpha\beta}(E) = \sqrt{g_\alpha g_\beta} \sum_{j=\pm 1} v_\alpha^j(\zeta) v_\beta^j(\zeta) \left| \frac{\partial \varepsilon_j}{\partial \zeta} \right|^{-1} \rho_0(\zeta) \Big|_{\zeta=\bar{\zeta}_j(E)}, \quad (6)$$

where  $\bar{\zeta}_j(E)$  is the inverse function of  $\bar{\varepsilon}_j(E)$ . The number of electrons in the state  $\alpha$  is

$$n_\alpha = 2 \int_{\mu_{\min}}^{\mu} dE \rho_{\alpha\alpha}(E, n_\alpha, n_b), \quad (7)$$

where  $\mu_{\min} = \bar{\varepsilon}_1(\zeta = -1)$  (note that  $\rho_{\alpha\beta}$  depends on  $n_\alpha$  through the functions  $g_\alpha$ ). The total number of charge carriers per site is  $n = \sum_\alpha n_\alpha(\mu)$ . This equality, along with Eqs. (4)–(7), form a set of equations for the calculation of  $n_\alpha$  and  $\mu$ . Performing a transformation of the operators  $a_\alpha$  employing the coefficients (5), we can find the Green's functions corresponding to the band spectrum (4) and derive the DOS,  $\rho_j$  for two  $j$ -bands

$$\rho_j(E) = \left[ \sum_\alpha g_\alpha [v_\alpha^j(\zeta)]^2 \right] \left| \frac{\partial \varepsilon_j(\zeta)}{\partial \zeta} \right|^{-1} \rho_0(\zeta) \Big|_{\zeta=\bar{\zeta}_j(E)}. \quad (8)$$

*Band structure and density of states.*— Superconducting cuprates vary from strongly anisotropic to nearly isotropic materials. To account for this, we consider two limiting cases: two-dimensional square and 3D cubic symmetries. The obtained results are quite similar and below we present the band structure and DOS (Figs. 1 and 2) calculated using Eqs. (4) and (8) only for the case of simple cubic lattice. Two very different quasiparticle spectra are shown in the insets of Figs. 1a,b. The anticrossing of two bands shown in the inset in Fig. 1a corresponds to a metallic behavior for any doping. When doping increases, the chemical potential  $\mu$  (shown by the dotted green line) shifts upward: at low doping we have one metallic band and one empty band; then two metallic bands; by further increasing the doping, one metallic and one filled band. For larger interband hybridization,  $t^{pd} > \sqrt{t^{pp}t^{dd}}$ , we obtain a transition to insulator at some doping level. Indeed, for some doping,  $\mu$  is located in the gap between zones. Nearby the anticrossing point of the two bands, the spectrum  $\varepsilon_j(\zeta(\mathbf{k}))$  becomes flatter. This could indicate the so-called nesting of the Fermi surface. For energies close to anticrossing points, the DOS exhibit peaks (Fig. 1), which are large,  $\rho_j \propto 1/\sqrt{E_0 - E}$ , when  $n$  is close to 1 in the vicinity of the metal-insulator transition (Fig. 1b). The optimal doping for superconductivity corresponds to the case when  $\mu$  is close to the energy where the peak of the DOS is observed.

*Phase separation in cuprates.*— The energy,  $E_{\text{hom}}(n) = 2 \sum_j \int_{\mu_{\min}}^{\mu} dE E \rho_j(E)$ , of the homogeneous state, versus doping  $n$ , is shown in the inset of Fig. 2a. The curvature of  $E_{\text{hom}}(n)$  is negative between the two marked points  $n_1$  and  $n_2$ . This indicates the instability of the homogeneous state with respect to the separation into two phases with hole densities  $n_1$  and  $n_2$ ,  $n_1 < n < n_2$  (see, e.g., Ref. 16). The energy  $E_{\text{ps}}(n) = c E_{\text{hom}}(n_1) + (1 - c) E_{\text{hom}}(n_2)$  of the PS state with relative phase fractions  $c$  and  $1 - c$ , which are determined by the charge conservation condition  $n = c n_1 + (1 - c) n_2$ , is lower than  $E_{\text{hom}}(n)$  between  $n_1$

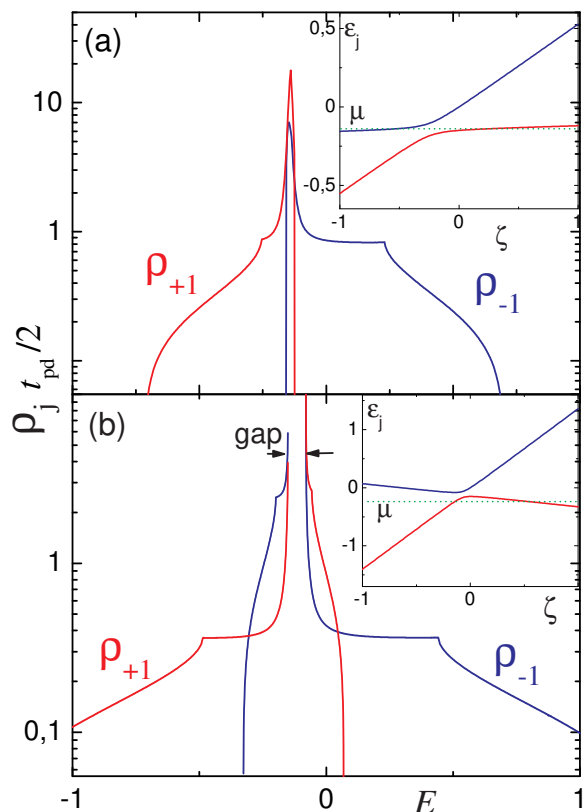


FIG. 1: (Color online) Density of states  $\rho_{\pm 1}$  versus energy  $E$  for quasiparticles (holes) located in bands  $j = \pm 1$  for two different types of spectra, shown in the corresponding insets. The gapless spectrum shown in the inset (a) was calculated at  $n = 0.6$ ,  $\varepsilon_d = 0.15$  eV,  $w_{pp} = 1$  eV,  $w_{dd} = 0.1$  eV, and relatively small interband hybridization  $w_{pd} = 0.25$  eV. The gapped spectrum in the inset (b) was calculated for the same parameters but for stronger interband hybridization  $w_{pd} = 1$  eV. In case (b), the transition to the insulating state occurs at a certain doping level for which the chemical potential  $\mu$  (shown by the green dotted line) is located inside the gap. In both cases, a large peak in the DOS is observed at energies corresponding to the anticrossing of the bands, where a significant flattening of the Fermi surface (see insets) takes place. The quasiparticle energy spectra are shown in the insets as a function of the variable  $\zeta$ , since  $\varepsilon_j$  depends on the crystal momentum  $\mathbf{k}$  only through  $\zeta(\mathbf{k})$ .

and  $n_2$  (see dashed line in the inset of Fig. 2). Thus, in a wide parameter range, the hole concentration  $n_2$  occurs near the optimum value. A typical dependence of the phase concentration  $c$  versus doping is shown in the inset of Fig. 2b. For low doping, the system is in a homogeneous state ( $c = 1$ ). If  $n > n_1$ , the sample divides into droplets with two different hole concentrations,  $n_1$  and  $n_2$ . Further increasing  $n$ , the relative concentration  $c$  of the phase with lower hole content  $n_1$  decreases almost linearly, and when  $n > n_2$  this phase disappears and the system becomes homogeneous again.

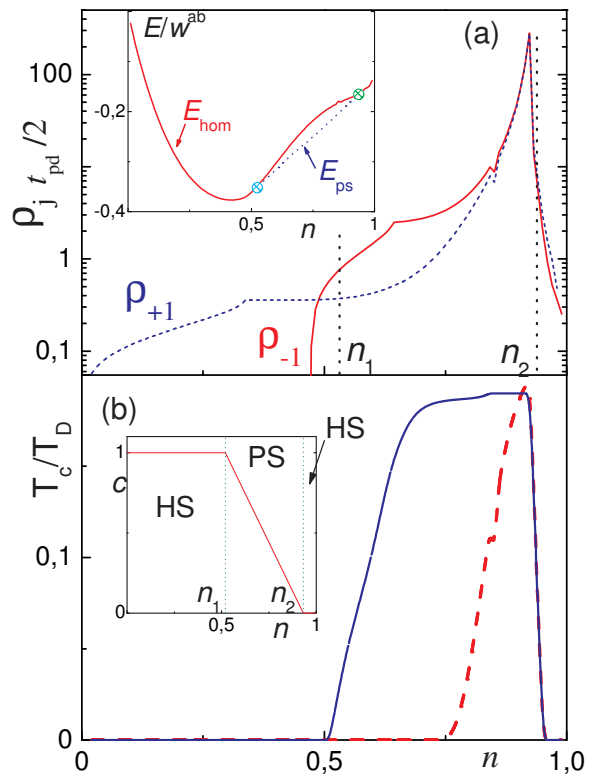


FIG. 2: (Color online) (a) The density of states at the Fermi level versus doping in the two-band Hubbard model. Inset in (a): energy of the homogeneous (red solid line) and the phase separated (blue dashed line) states. The dependence of the energy in the homogeneous state,  $E_{\text{hom}}$ , on  $n$  has a negative curvature if  $n_1 < n < n_2$ . In this range of doping, the PS state becomes more favorable since its energy,  $E_{\text{ps}}$ , is lower than  $E_{\text{hom}}$  (see inset in (a)). The values  $n_{1,2}$  are indicated in the main panel of (a) by black vertical dotted lines. The point  $n_2$  is near the peak in the DOS. (b) The critical temperature,  $T_c$ , of the superconducting transition versus doping level  $n$  for the homogeneous (red dashed line) and PS (blue solid line) states calculated using Eq. (9). The  $T_c(n)$  of the homogeneous state decreases fast when the doping  $n$  deviates from its optimum value about  $n_2$ . In contrast to this,  $T_c(n)$  in the PS state is a broad function and exhibits a plateau within the  $n_1 < n < n_2$  range. Inset in (b) demonstrates the dependence of the concentration  $c$  of the phase with lower hole content versus  $n$ . The regions of homogeneous (HS) and PS states are indicated in the inset. Here we use the following parameters:  $\varepsilon_d = 0.2$  eV,  $w_{pp} = 1$  eV,  $w_{dd} = 0.3$  eV, and  $w_{pd} = 0.7$  eV.

Further analysis shows that the PS state occurs in the parameter range where  $w_{pd} < w_{pp}$ . If  $w_{pd} \gg w_{pp}$ , the two-band Hubbard Hamiltonian reduces to an effective single-band model, as is commonly accepted [10, 12] and the discussed cause for PS in the system disappears.

The PS leads to a redistribution of the charge carriers and charge neutrality breaking. The structure of the PS state can be either ordered (e.g., checkerboard structure) or random (i.e., randomly distributed droplets of one

phase within a matrix of the other phase). For the random PS state, the size ( $D$ ) of the droplet is determined by the competition between the Coulomb and surface energies. Following the approach developed in Ref. 16, we can estimate  $D$  as  $(3 - 6)d$  at  $w_{pd} \sim w_{pp} \sim 1$  eV, in agreement with the experimental data in [2], where spatial variations of the DOS and superconducting gap were measured using STM.

*Critical temperature versus doping.*— Hereafter we do not focus on a precise mechanism of superconductivity in cuprates. Instead, we intend to analyze the effect of the two-band structure of the Hubbard Hamiltonian (1) and PS on the critical temperature  $T_c$  of the superconducting transition. To estimate  $T_c$  we now use the BCS formula [18] accounting for the Coulomb repulsion

$$T_c = T_D \exp[-1/(\rho_j V_p - \nu_c)], \quad (9)$$

where  $T_D$  is the Debye temperature,  $V_p$  is the BCS electron-phonon coupling constant,  $\nu_c = \rho_j V_c / [1 + \rho_j V_c \ln(\mu/k_B T_D)]$  is the Coulomb pseudo-potential, and  $V_c \sim U^p \approx 5$  eV are the Coulomb matrix elements. In our approach, the homogeneous state superconductivity can appear in different bands depending on doping, see Fig. 1: in band  $j = 1$  for low doping and in  $j = -1$  for higher doping. We stress that this is consistent with the superconducting behavior of YBCO where superconductivity switches from 60 K to 90 K with increasing the oxygen content. For intermediate doping, the superconducting state can simultaneously coexist in two bands, as in MgB<sub>2</sub>. Our model could also be used to interpret experiments [19] showing the existence of PS in MgB<sub>2</sub>. However, a direct application of our studies for MgB<sub>2</sub> should be justified since it is not clear whether the Hubbard-like description is applicable to this compound.

The dependence of  $T_c$  on doping  $n$  for the homogeneous state is shown by the dashed line in Fig. 2b. For the optimum doping level, corresponding to the anticrossing point (see insets in Fig. 1) of two hole energies,  $T_c$  reaches its maximum because of the peak in the DOS. Away from optimal doping,  $T_c(n)$  decreases fast with  $n$ . In the PS state, one of the phases retains the optimum hole concentration within a wide interval of doping levels. This results in a slower decrease (see blue solid line in Fig. 2b) of  $T_c$  when  $n$  deviates from the optimal value  $n_2$ . This provides a possible natural explanation of the observed  $T_c$  dependence on hole doping in cuprates.

*Conclusions.*— We studied the two-band Hubbard model for superconducting cuprates and other multiband superconductors. Using the Green's functions technique, we calculated the hole band structure and the density of states at the Fermi level. The density of states exhibits a large peak at the anticrossing of hole bands. The peak is due to the flattening of the Fermi surface. Near this doping level, a transition from metal to insulator can occur. Due to the peak in the density of states,  $T_c$  can significantly increase. For a certain range of the model

parameters, a spatial phase separation of the hole carriers between the two Hubbard bands was found. The discussed mechanism of PS is an alternative to the usual explanation of the PS, which is attributed to strong antiferromagnetic correlations (see, e.g., [1, 9]). Our estimates of the spatial scale of PS is in a good agreement with important experimental results [2]. Using the BCS expression for  $T_c$ , also accounting for Coulomb repulsion, we show that  $T_c(n)$  is near its maximum within the doping range where PS occurs.

We acknowledge stimulating discussions with A.V. Rozhkov and partial support from the NSA, LPS, ARO, NSF (grant No. EIA-0130383), JSPS-RFBR (grant No. 06-02-91200), CTC program supported by JSPS, RFBR (grants No. 06-02-16691 and 05-02-17600), MEXT Grant-in-Aid No. 18740224, the EPSRC grant No. EP/D072581/1), and EU project CoMePhs.

- 
- [1] E. Dagotto, *Science* **309**, 257 (2005).
  - [2] K.M. Lang *et al.*, *Nature (London)* **415**, 412 (2002).
  - [3] J.E. Hoffman *et al.*, *Science* **295**, 466 (2002).
  - [4] M. Vershinin *et al.*, *Science* **303**, 1995 (2004).
  - [5] L.P. Gor'kov and A.V. Sokol, *JETP Lett.* **48**, 547 (1987); J. Zaanen and O. Gunnarsson, *Phys. Rev. B* **40**, 7391 (1989); V.J. Emery *et al.*, *Phys. Rev. Lett.* **64**, 475 (1990).
  - [6] W.-F. Tsai and S.A. Kivelson, *Phys. Rev. B* **73**, 214519 (2006); G. Seibold *et al.*, *Phys. Rev. B* **58**, 13506 (1998).
  - [7] C.S. Hellberg and E. Manousakis, *Phys. Rev. Lett.* **78**, 4609 (1997); C.T. Shih *et al.*, *Phys. Rev. B* **57**, 627 (1998); T.-H. Gimm and S.-H. Suck-Salk, *Phys. Rev. B* **62**, 13930 (2000); W.O. Putikka and M.U. Luchini, *Phys. Rev. B* **62**, 1684 (2000).
  - [8] A. Macrìdin *et al.*, *Phys. Rev. B* **74**, 085104 (2006).
  - [9] E. Nagaev, *Colossal Magnetoresistance and Phase Separation in Magnetic Semiconductors* (Imperial College Press, London, 2002).
  - [10] *The Physics of Superconductors*, vol. II, edited by K.H. Benneman and J.B. Ketterson (Springer, Berlin, 2004).
  - [11] L.P. Gor'kov and G.B. Teitelbaum, *Phys. Rev. Lett.* **97**, 247003 (2006).
  - [12] V.J. Emery, *Phys. Rev. Lett.* **58**, 2794 (1987); F.C. Zhang and T.M. Rice, *Phys. Rev. B* **37**, 3759 (1988).
  - [13] J.B. Goodenough, *Europhys. Lett.* **57**, 550 (2002).
  - [14] L. Hozoi *et al.*, *Phys. Rev. B* **72**, 144510 (2005); L. Hozoi and S. Nishimoto, *ibid* **73**, 245101 (2006).
  - [15] A non-zero average  $\langle a_{\alpha}^{\dagger} a_{\bar{\alpha}} \rangle$  is a well-known internal inconsistency of the Hubbard I approximation at  $t_{ab} \neq 0$  [17] since it produces a non-Hermitian behavior of the Green functions. However, for the parameter range discussed here, these values are small compared to the coefficients  $g_{\alpha}$  that characterize the maximum band filling in our model,  $|\langle a_{\alpha}^{\dagger} a_{\bar{\alpha}} \rangle|^2 \ll g_{\alpha} g_{\bar{\alpha}}$ . It can be shown that under the latter condition the effect of  $\langle a_{\alpha}^{\dagger} a_{\bar{\alpha}} \rangle$  on the band structure and band filling is negligible.
  - [16] K.I. Kugel, A.L. Rakhmanov, and A.O. Sboychakov, *Phys. Rev. Lett.* **95**, 267210 (2005); A.O. Sboychakov, A.L. Rakhmanov, and K.I. Kugel, *Phys. Rev. B* **74**,

- 014401 (2006).
- [17] J. Hubbard, Proc. Roy. Soc. (London) **A281**, 401 (1964).
- [18] P.G. de Gennes, *Superconductivity of Metals and Alloys* (Perseus Books, New York, 1999).
- [19] D.N. Arcos and M.N. Kunchur, Phys. Rev. B **71**, 184516 (2005).